APL Photonics

Observing mode-dependent wavelength-to-time mapping in few-mode fibers using a single-photon detector array

Cite as: APL Photonics **5**, 061303 (2020); https://doi.org/10.1063/5.0006983
Submitted: 09 March 2020 . Accepted: 10 May 2020 . Published Online: 09 June 2020

Harikumar K. Chandrasekharan, Katjana Ehrlich, Michael G. Tanner, Dionne M. Haynes, Sebabrata Mukherjee, Tim A. Birks, and Robert R. Thomson

AIP Publishing

Observing mode-dependent wavelength-to-time mapping in few-mode fibers using a single-photon detector array

Cite as: APL Photon. 5, 061303 (2020); doi: 10.1063/5.0006983
Submitted: 9 March 2020 • Accepted: 10 May 2020 •
Published Online: 9 June 2020

Harikumar K. Chandrasekharan,[1,a] Katjana Ehrlich,[1,2] Michael G. Tanner,[1] Dionne M. Haynes,[3,b] Sebabrata Mukherjee,[4] Tim A. Birks,[5] and Robert R. Thomson[1]

AFFILIATIONS

[1]Scottish Universities Physics Alliance (SUPA), Institute of Photonics and Quantum Sciences, Heriot-Watt University, Edinburgh EH14 4AS, United Kingdom
[2]Centre for Inflammation Research, Queen's Medical Research Institute, University of Edinburgh, 47 Little France Crescent, Edinburgh EH16 4TJ, United Kingdom
[3]Leibniz Institute for Astrophysics Potsdam, An der Sternwarte 16, D-14482 Potsdam, Germany
[4]Department of Physics, The Pennsylvania State University, University Park, Pennsylvania 16802, USA
[5]Department of Physics, University of Bath, Claverton Down, Bath BA2 7AY, United Kingdom

[a]**Author to whom correspondence should be addressed:** hk47@hw.ac.uk
[b]**Current address:** Research School of Astronomy and Astrophysics, Australian National University, Canberra, ACT 2611, Australia.

ABSTRACT

Wavelength-to-time mapping (WTM)—stretching ultrashort optical pulses in a dispersive medium such that the instantaneous frequency becomes time-dependent—is usually performed using a single-mode fiber. In a number of applications, such as time-stretch imaging (TSI), the use of this single-mode fiber during WTM limits the achievable sampling rate and the imaging quality. Multimode fiber based WTM is a potential route to overcome this challenge and project a more diverse range of light patterns. Here, we demonstrate the use of a two-dimensional single-photon avalanche diode (SPAD) array to image, in a time-correlated single-photon counting (TCSPC) manner, the time- and wavelength-dependent arrival of different spatial modes in a few-mode fiber. We then use a TCSPC spectrometer with a one-dimensional SPAD array to record and calibrate the wavelength-dependent and mode-dependent WTM processes. The direct measurement of the WTM of the spatial modes opens a convenient route to estimate group velocity dispersion, differential mode delay, and the effective refractive index of different spatial modes. This is applicable to TSI and ultrafast optical imaging, as well as broader areas such as telecommunications.

There is currently a global drive to develop new techniques and technologies capable of imaging phenomena with ultrafast (sub-nanosecond) timing resolutions. The applications for such techniques range from fundamental physics,[1,2] such as the study of how relativistic processes affect image creation, to future real-world applications such as three-dimensional LIDAR[3,4] and high-throughput imaging of cells.[5] One of the key ultrafast imaging techniques that has been developed over the past decade is time-stretch imaging (TSI). In TSI, a short (usually femtosecond or picosecond) spectrally broad pulse of light is spatially dispersed across an object (a so-called "spectral shower"), for example, by using prisms or gratings. The wavelength modulated pulse is then subjected to a large amount of chromatic dispersion to temporally stretch and chirp the pulses. After this process, the instantaneous wavelength of the pulse rapidly changes as a function of time across the pulse—a process known as wavelength-to-time mapping (WTM).[6–8] The spatially varying optical properties (e.g., transmission) of the object will then be imprinted on the temporal profile of

the pulse, which can then be detected using a single fast detector. In comparison to other ultrafast imaging techniques, which use gated or pump–probe approaches, each time-stretched pulse provides a full image of the scene. As such, TSI is uniquely well-suited to imaging non-repetitive events with high frame rates (up to the gigahertz regime) and short frame exposures limited only by the duration of the pulse scene.

Currently, the WTM function of any TSI system is almost always performed using a single-mode optical fiber.[9] In this case, each wavelength within the pulse is guided by an LP_{01} mode, which then samples a similarly shaped region of the scene. This limits the sampling of the scene and fundamentally limits the imaging quality that can be achieved. One promising route to overcome this limitation is to exploit multimode optical fibers[10–12] to project a more diverse range of light patterns onto the scene. Examples of approaches currently being pursued in this area include using a highly multimode fiber to convert a single-mode time-stretched pulse into a rapidly varying pattern of light that can then be projected onto the scene, the data from which can then be processed using compressive sensing algorithms.[13] Another promising approach is to use a few-mode fiber (FMF) for the time-stretch process itself.[14] In this case, each mode can be used to sample the scene in a slightly different way, resulting in multiple images which could then, in principle, be combined to enable higher quality images.

Regardless of which route eventually proves to be optimum for a particular application, a key capability for future multimode TSI techniques is the precise calibration of how the output of the multimode fiber varies with time and wavelength. Mode-dependent WTM in few-mode fibers was previously demonstrated utilizing single photodetectors and sampling oscilloscopes.[15,16] More recently, a single pixel camera based on a single detector and a digital micro-mirror device (DMD) was demonstrated to observe the temporal evolution of mode patterns at single wavelengths in an FMF and an orbital angular momentum mode conserving optical fiber.[17] However, in this paper, we demonstrate that complementary metal-oxide-semiconductor (CMOS) single-photon avalanche diode (SPAD) arrays provide a powerful multiplexed technology to perform detailed WTM calibrations across a broad wavelength range. More specifically, we are using a two-dimensional CMOS SPAD array with 32 × 32 pixels, each with its independent timing electronics, and, therefore, capable of highly multiplexed time-correlated single-photon counting (TCSPC) to directly image the arrival of different spatial modes in an FMF. We then use a time-resolving spectrometer, based on a one-dimensional CMOS SPAD array with the same multiplexed TCSPC capability, to demonstrate broadband observation of the mode-dependent and wavelength-dependent WTM processes in an FMF.

The experimental setup we used to image the time-resolved arrival of the different spatial modes in a fiber is shown in Fig. 1. SMF-28 fiber is used which has a core diameter of ≈8.2 μm and an NA of 0.14. It is designed to be single-mode at $\lambda = 1310$ nm but supports between six linearly polarized (LP) modes at 500 nm and five LP modes at 610 nm, so it is used here as an FMF. The refractive index profile of the fiber exhibited a smooth core-cladding interface and a central dip (see Fig. 1 in the supplementary material), which are important for mode propagation behavior.[15,18]

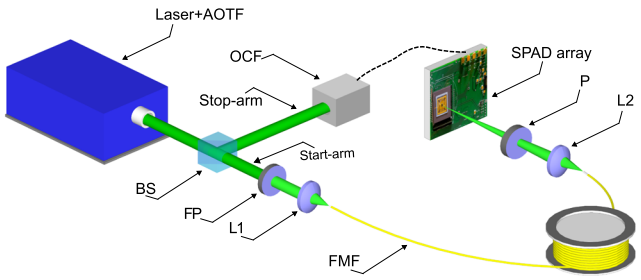

FIG. 1. Experimental setup for the light-in-flight spatial mode-imaging system. Two different arms enable TCSPC measurements. In the start-arm, the signal from the fiber starts the TCSPC timer on the SPAD array, while the periodic trigger signal from the laser stops the TCSPC measurement in the stop-arm.

Spectrally narrow tunable pulses of light were selected from the broadband output of a supercontinuum laser (SuperK EXTREME EXW-12, NKT Photonics, pulse repetition rate =19.5 MHz) using an acousto-optic tunable filter (AOTF) in combination with an angle-tunable Fabry–Pérot (FP) filter (Delta Optical Thin Films). The AOTF covers a wavelength range from 455 nm to 700 nm, with a passband bandwidth ranging from 2.5 nm to 8.5 nm, respectively. The spectral power of the light after the AOTF output within the 500–600 nm wavelength range was measured to be ≈2 mW/nm, with a pulse repetition rate of 78 MHz. The FP filter was used to further reduce the bandwidth of the light after the AOTF, narrowing the full width at half maximum (FWHM) to ≈1 nm. The central wavelength of these pulses was measured after the FP filter using a commercial spectrometer (QE Pro, Ocean Optics Inc.). Due to the narrow spectral bandwidth of the pulses, temporal broadening due to chromatic dispersion is minimized, and the temporal resolution of the SPADs is sufficient to resolve the arrival of the individual spatial modes. The filtered light from the FP filter was focused onto one end of a 981.5 m long length (measured using an optical time domain reflectometer) of the FMF (SMF-28) using a lens L1 (f = 8 mm). The output of the FMF was imaged using lens L2 (f = 4.51 mm) onto a two-dimensional multipixel SPAD array (Megaframe 32), which consists of a 32 × 32 array of SPADs spaced on a 50 × 50 μm^2 square grid.[19] Each SPAD has a photosensitive area of ≈6 μm in diameter. Crucially, for our application, each pixel has a dedicated time-to-digital converter (TDC) for independent TCSPC with a dynamic range of 54 ns and a timing bin duration of ≈53 ps.[20,21] The TCSPC imaging capability and sensitivity of the Megaframe SPAD array have recently resulted in the realization of key demonstrations in applied and fundamental physics.[22–25]

For TCSPC, the arrival times of photons are measured as differences between start and stop signals. To reduce the overhead on the timing electronics and enable fast acquisition times, the SPAD array is configured to work in the "reverse start–stop" mode,[26] where the detection of a single photon by any SPAD starts the clock on its specific TDC. The clock then stops when it receives a stop signal, which for our purposes was generated by directing a portion of the light from the laser onto an optical constant fraction (OCF) discriminator. Due to the variability in the individual TDCs for each SPAD, the full width at half maximum instrument response function (IRF) was found to vary from 137 ps to 174 ps, with a standard deviation

of ±18 ps. Furthermore, because the stop signal arrives at different times to the TDCs across the SPAD array, the TCSPC signals are aligned non-uniformly across the pixels.[24] This shift was taken into account and corrected for during the post-processing of the data.

Figure 2 (Multimedia view) presents the imaging data obtained from the SPAD array using the light centered at 532 nm with a full width at half maximum (FWHM) bandwidth of ≈1 nm. To reduce the temporal broadening of the signal at the detector due to degenerative LP modes, a polarizer (P) was used just after the output imaging lens L2. In the experiments, we obtain the spatial intensity distribution as a function of time; Fig. 2(a) shows the summed counts in each pixel for the entire duration of the TCSPC trace (51 ns, the laser pulse period), while Fig. 2(b) shows the time evolution of the signal acquired for two representative pixels in which well resolved peaks are observed. The spatial intensity profile of the LP modes is then simply obtained by identifying the peaks in the intensity pattern [Fig. 2(b)]; Fig. 2(c) shows normalized images of the spatial intensity distributions summed over the peaks in Fig. 2(b), and the title of each frame represents the peak arrival time of the mode pattern. The six distinct mode patterns are recognizable as the LP modes supported by the fiber, which are, thus, labeled on the peaks in Fig. 2(b). The fiber is wrapped firmly on a fiber drum to minimize time-varying disturbances of the fiber during the measurements. This minimizes phase variations between modes during the measurement, enabling us to record the easily recognizable mode patterns we report.

Due to chromatic dispersion, the light contained in each mode is observed to arrive over a ≈420 ps window. At 532 nm, the LP_{01} mode propagates faster and arrives at the SPAD array first. This is then followed by the LP_{12}, LP_{11}, LP_{02}, LP_{21}, and LP_{31} modes, indicating that the group index of the modes is higher for successive modes. The time difference between the slowest (LP_{31}) and the fastest mode (LP_{01}) (maximal excursion) in a differential group delay is ≈5.5 ns.

The time-resolved mode-imaging process was repeated using pulses of light with a range of central wavelengths from 500 nm to 610 nm which were selected using the AOTF in combination with the angle-tunable FP filter. Figure 3(a) presents the measured (symbols) relative arrival times for six spatial modes recorded on one pixel of the SPAD array. To minimize the measurement fluctuations, a locally weighted regression (LOESS) is used to smooth the data, shown as the trend lines. Based on the arrival time of photons, the values of chromatic dispersion[27] for the six modes were calculated from the smoothed data and are given in Fig. 3(b).

Based on the arrival times of the photons, the chromatic dispersion at a wavelength (λ) in different LP modes was calculated using the formula $D_\lambda = (T_{\lambda+\Delta\lambda/2} - T_{\lambda-\Delta\lambda/2})/(\Delta\lambda L)$, where T_λ is the arrival time of photons with wavelength λ, $\Delta\lambda$ is the increment in wavelength, and L is the length of the fiber. As is conventional, we express the chromatic dispersion in units of ps/nm/km.

The mode-imaging results can be used to calculate the relative modal delay with respect to the fundamental mode. Figure 4(a) shows the experimentally observed (symbols) relative modal delay of

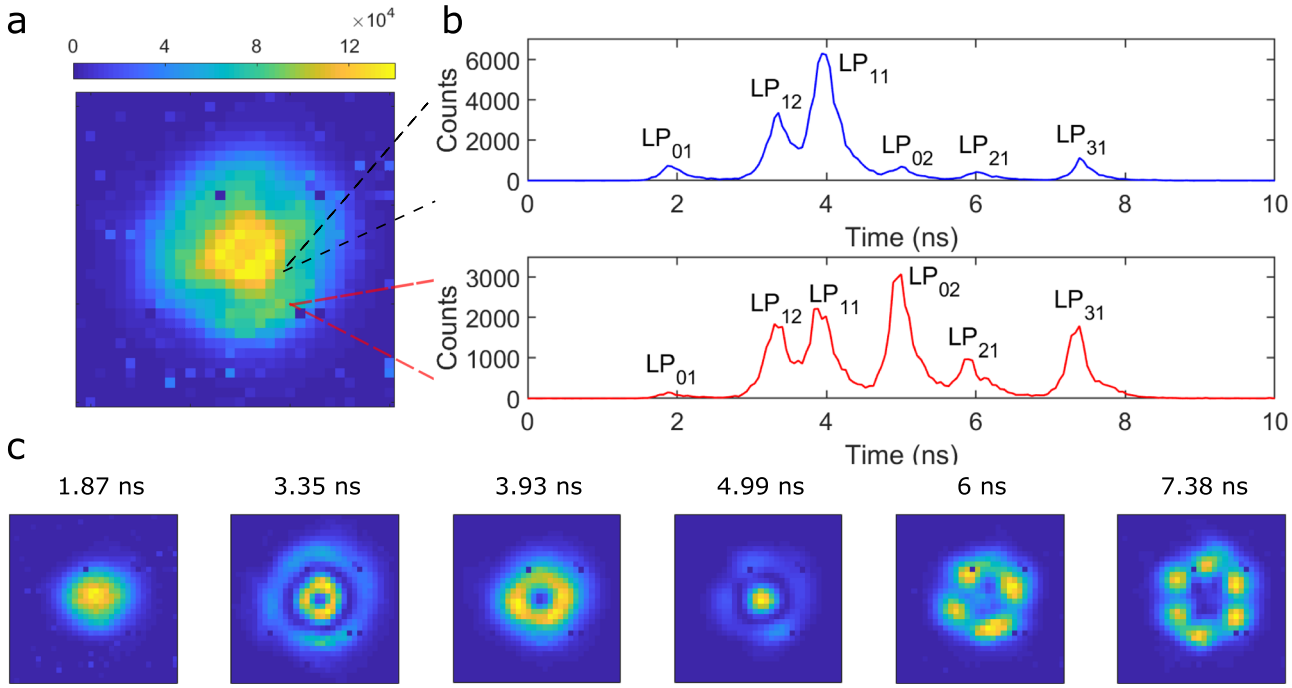

FIG. 2. (a) Recorded optical intensity distributions in the entire SPAD array field of view summed over the entire measurement period (10 ns); the color bar represents photon counts. (b) Two representative pixels showing intensity variation over time with six peaks observed. (c) Evolution of the normalized spatial intensity distribution at the SPAD array with peak arrival times. The observed peaks in (b) are labeled the modes LP_{01}, LP_{12}, LP_{11}, LP_{02}, LP_{21}, and LP_{31}, identified from patterns in (c). Multimedia view: https://doi.org/10.1063/5.0006983.1

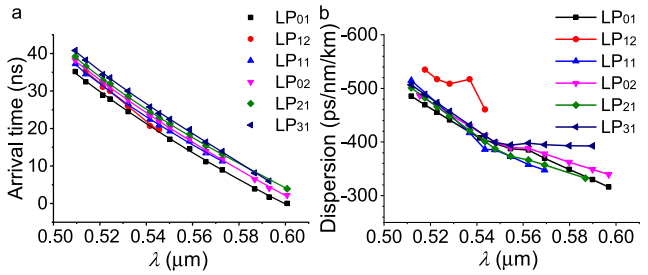

FIG. 3. (a) Relative arrival times of photons at the SPAD array for six spatial modes as functions of wavelength. Symbols show measurement data and smoothed trend lines are generated with a locally weighted regression. (b) Measured chromatic dispersion of the modes as a function of wavelength.

five spatial modes compared to the LP_{01} mode as a function of wavelength. The SPAD array provides time- and spatially resolved intensity information. This allows each peak in the histogram obtained for each SPAD to be attributed to an LP spatial mode supported by the fiber. Using this information, the relative delay of each spatial mode relative to the fundamental mode can be trivially obtained from $T_{LP} = T_{LP} - T_{01}$, where T_{LP} is the arrival time of the LP mode in question and T_{01} is the arrival time of the fundamental mode (LP_{01}), respectively. The numerically obtained modal delay (solid lines) is also shown, calculated using the scalar wave equation for a fiber[10–12,15] and the radial refractive index profile measured for the fiber used in the experiments.

The effective refractive index differences of the modes can also be calculated from the mode-imaging results. Based on the refractive index profile, Fig. 4(b) represents the differences in the effective indices of the closest modes ($\Delta\eta_{\text{eff}}$). Both the numerical (solid) and experimental values (symbols) match well. The measured refractive index differences are in the order of 10^{-4}, which is comparable with measurements offered by interferometric techniques.[28] Unlike interferometry, the time-resolved imaging technique does not require complicated calibration or careful measurement accuracy, which makes the system feasible for future applications. Our numerical calculations indicate that the relatively small discrepancy between the experimental data and numerically obtained results in

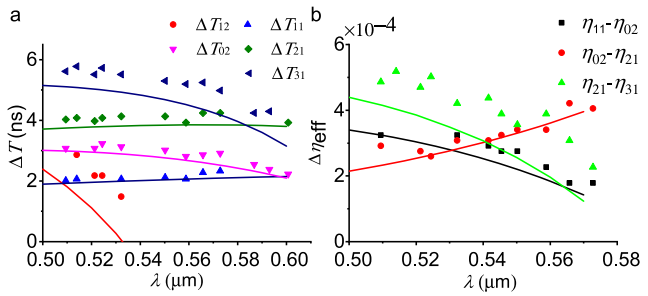

FIG. 4. (a) Relative modal delay between different mode groups with respect to the LP_{01} mode. The solid lines represent the numerical modal delay difference, and the marked points represent the experimental results. (b) Numerical (solid lines) and experimental (marked) effective refractive index differences between the closest mode groups. In addition, see Fig. 2 in the supplementary material.

Fig. 4 can be caused by differences between the true and experimentally measured refractive index profiles of the fiber due to the limitations of the experimental apparatus (see the supplementary material).

The results presented so far have demonstrated the potential of using two-dimensional SPAD arrays to calibrate the wavelength-dependent and time-dependent patterns generated in TSI systems exploiting multimode and few-mode fibers. We also anticipate that future multimode TSI systems will exploit spectrometers with ultrafast detectors to record in real time how the scene modulates the signal for each mode at each wavelength. Here, we demonstrate how multiplexed SPAD arrays can be used to calibrate the WTM process in multimode fibers. To perform these measurements, the AOTF and FP were removed from the start-arm of the experimental setup shown in Fig. 1 and the FP was replaced by a filter set that passes light in the 500–700 nm spectral range. The broadband transmitted light was then coupled to the FMF. The output of the FMF was butt-coupled to a multimode fiber (FG050LGA, Thorlabs), which acted as an input slit to a TCSPC spectrometer.[29,30] The spectrometer consists of a transmission volume grating (600 grooves/mm, Wasatch) and a SPAD line array with 256 pixels.[29] Again, each SPAD has its own TDC facilitating independent TCSPC in a reversed start–stop TCSPC modality.[31,32] The TDC resolution of this SPAD array is 420 ps, and the IRF of the SPADs is 0.6 ns. This limits the resolution of the individual LP modes in the time domain. Each pixel detects light with a bandwidth of 5 nm.

Figure 5 presents the wavelength-resolved TCSPC data taken across the spectral range in a single fast measurement. The overlaid data points are the spatial mode arrival times recorded with the imaging SPAD array [same data points presented in Fig. 3(a)]. The energy distribution between the modes and the wavelengths is extremely sensitive to the coupling conditions, position on the fiber endface, and incident angle, so the intensities observed over the peak arrival time evolution of the LP modes are significantly different

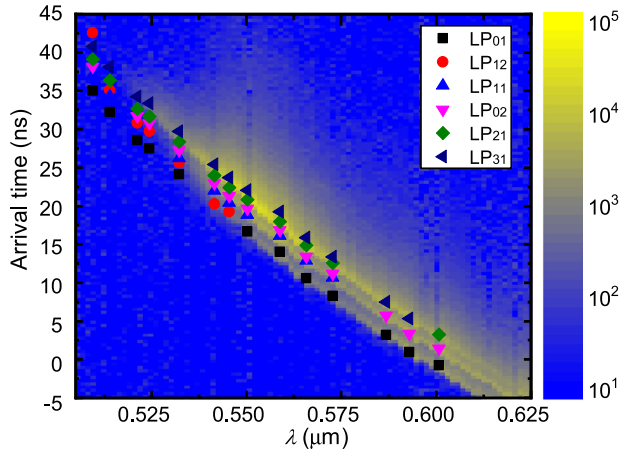

FIG. 5. Arrival time of photons recorded with broadband illumination and the SPAD line sensor. The color bar represents photon counts. The marked data points represent the measured arrival times of spatial modes recorded with the imaging SPAD array [same data points in Fig. 3(a)].

compared to the results shown in Fig. 2. The evolution of modes resembles the experimental findings from Fig. 3(a). The total difference in the arrival time between 520 nm and 600 nm is 30 ns. For shorter wavelengths, the peak arrival times broaden as more modes appear. However, due to the lower time resolution of the line sensor, we are not able to resolve all six LP modes. Regardless, our results demonstrate the feasibility of using future time-resolved spectrometers with optimized SPAD arrays to precisely calibrate the wavelength-dependent and mode-dependent WTM processes in multimode fibers.

To maximize the number of modes that can be observed by our current system, a future experiment would aim at using a length of fiber that generates a mode delay between the slowest and fastest propagating modes equal to the temporal dynamic range of the SPAD array (54 ns) and a minimum intermodal delay between two temporally adjacent modes equal to the instrument response function (150 ps). Our simulations indicate that a 3.5 km length of fiber with a core-cladding refractive index contrast of 0.0055 and a core radius of 11 μm would satisfy these requirements while supporting the guidance of 27 modes. This indicates that our current system should be capable of observing at least 27 modes, but this can be increased in the future through the use of improved SPAD arrays.

In conclusion, we have demonstrated new approaches to observe, investigate, and calibrate WTM processes in multimode fibers using multipixel two-dimensional and line array CMOS SPAD sensors. The demonstrated results provide new and easy to implement methods to calculate the group velocity dispersion (GVD) and differential mode delay (DMD) of different spatial modes and the effective refractive index difference between the closest mode groups in the FMF from the wavelength-dependent arrival times of photons. The measured refractive index differences are in the order of 10^{-4}, which is comparable with current interferometric techniques. The multiplexing capability of the instrument was demonstrated over a broad range of wavelengths from 520 nm to 600 nm. By carefully selecting fiber parameters and detector design, this technique can also offer simultaneous measurements of GVD and DMD over a broad wavelength region for optical telecommunication applications. The direct observation of time evolution and the WTM of the spatial modes will find applications in areas such as time-stretch microscopy, optical telecommunication, real-time soliton imaging, and ultrafast optical imaging.

SUPPLEMENTARY MATERIAL

See the supplementary material for the measured refractive index profile and the relative modal delay calculation.

ACKNOWLEDGMENTS

The authors thank R. K. Henderson (U. of Edinburgh) for providing the Megaframe 32 and the CMOS SPAD line array used in this work, the latter of which was developed through the EPSRC "Proteus" project (Grant No. EP/K03197X/1). H.K.C. and K.E. thank Heriot-Watt University for support in the form of James Watt Ph.D. scholarships.

DATA AVAILABILITY

The data that support the findings of this study are openly available in the Heriot-Watt University PURE research data management system.[33]

REFERENCES

[1] M. Clerici, G. C. Spalding, R. Warburton, A. Lyons, C. Aniculaesei, J. M. Richards, J. Leach, R. Henderson, and D. Faccio, "Observation of image pair creation and annihilation from superluminal scattering sources," Sci. Adv. **2**(4), e1501691 (2016).
[2] H. Defienne, M. Reichert, J. W. Fleischer, and D. Faccio, "Quantum image distillation," Sci. Adv. **5**(10), eaax0307 (2019).
[3] J. Tachella, Y. Altmann, N. Mellado, A. McCarthy, R. Tobin, G. S. Buller, J.-Y. Tourneret, and S. McLaughlin, "Real-time 3D reconstruction from single-photon lidar data using plug-and-play point cloud denoisers," Nat. Commun. **10**, 4984 (2019).
[4] A. Turpin, G. Musarra, F. Tonolini, R. Murray-Smith, and D. Faccio, "Single photon and single pixel technology for computational lidar," in *Laser Congress 2019 (ASSL, LAC, LS&C)* (Optical Society of America, 2019), p. LTh2B.2.
[5] K. Goda, K. K. Tsia, and B. Jalali, "Serial time-encoded amplified imaging for real-time observation of fast dynamic phenomena," Nature **458**, 1145 (2009).
[6] L. G. Cohen and C. Lin, "Pulse delay measurements in the zero material dispersion wavelength region for optical fibers," Appl. Opt. **16**, 3136–3139 (1977).
[7] H. Chi and J. Yao, "Fiber chromatic dispersion measurement based on wavelength-to-time mapping using a femtosecond pulse laser and an optical comb filter," Opt. Commun. **280**, 337–342 (2007).
[8] T. Ito, O. Slezak, M. Yoshita, H. Akiyama, and Y. Kobayashi, "High-precision group-delay dispersion measurements of optical fibers via fingerprint-spectral wavelength-to-time mapping," Photonics Res. **4**, 13–16 (2016).
[9] T. T. W. Wong, A. K. S. Lau, K. K. Y. Ho, M. Y. H. Tang, J. D. F. Robles, X. Wei, A. C. S. Chan, A. H. L. Tang, E. Y. Lam, K. K. Y. Wong, G. C. F. Chan, H. C. Shum, and K. K. Tsia, "Asymmetric-detection time-stretch optical microscopy (ATOM) for ultrafast high-contrast cellular imaging in flow," Sci. Rep. **4**, 3656 (2014).
[10] E. Snitzer, "Cylindrical dielectric waveguide modes*," J. Opt. Soc. Am. **51**, 491–498 (1961).
[11] A. W. Snyder and W. R. Young, "Modes of optical waveguides," J. Opt. Soc. Am. **68**, 297–309 (1978).
[12] D. Gloge, "Weakly guiding fibers," Appl. Opt. **10**, 2252–2258 (1971).
[13] G. Wang, C. K. Mididoddi, F. Bai, S. Gibson, L. Su, J. Liu, and C. Wang, "Ultrafast optical imaging using multimode fiber based compressed sensing and photonic time stretch," arXiv:1803.03061.
[14] Y. Qiu, J. Xu, K. K. Y. Wong, and K. K. Tsia, "Exploiting few mode-fibers for optical time-stretch confocal microscopy in the short near-infrared window," Opt. Express **20**, 24115–24123 (2012).
[15] Y. Painchaud, P. LeBel, M. A. Duguay, and R. J. Black, "Time-resolved identification of modes and measurement of intermodal dispersion in optical fibers," Appl. Opt. **31**, 2005–2010 (1992).
[16] J. Cheng, M. E. V. Pedersen, K. Wang, C. Xu, L. Grüner-Nielsen, and D. Jakobsen, "Time-domain multimode dispersion measurement in a higher-order-mode fiber," Opt. Lett. **37**, 347–349 (2012).
[17] S. D. Johnson, D. B. Phillips, Z. Ma, S. Ramachandran, and M. J. Padgett, "A light-in-flight single-pixel camera for use in the visible and short-wave infrared," Opt. Express **27**, 9829–9837 (2019).
[18] W. Gambling, D. Payne, and H. Matsumura, "Effect of dip in the refractive index on the cut-off frequency of a single-mode fibre," Electron. Lett. **13**, 174–175 (1977).
[19] J. Richardson, R. Walker, L. Grant, D. Stoppa, F. Borghetti, E. Charbon, M. Gersbach, and R. K. Henderson, "A 32 × 32 50 ps resolution 10 bit time to digital converter array in 130 nm CMOS for time correlated imaging," in *2009 IEEE Custom Integrated Circuits Conference* (IEEE, 2009), pp. 77–80.

[20]M. Gersbach, Y. Maruyama, R. Trimananda, M. W. Fishburn, D. Stoppa, J. A. Richardson, R. Walker, R. Henderson, and E. Charbon, "A time-resolved, low-noise single-photon image sensor fabricated in deep-submicron CMOS technology," IEEE J. Solid-State Circuits **47**, 1394–1407 (2012).
[21]N. Krstajić, S. Poland, J. Levitt, R. Walker, A. Erdogan, S. Ameer-Beg, and R. K. Henderson, "0.5 billion events per second time correlated single photon counting using CMOS SPAD arrays," Opt. Lett. **40**, 4305–4308 (2015).
[22]S. P. Poland, N. Krstajić, J. Monypenny, S. Coelho, D. Tyndall, R. J. Walker, V. Devauges, J. Richardson, N. Dutton, P. Barber, D. D.-U. Li, K. Suhling, T. Ng, R. K. Henderson, and S. M. Ameer-Beg, "A high speed multifocal multiphoton fluorescence lifetime imaging microscope for live-cell FRET imaging," Biomed. Opt. Express. **6**, 277–296 (2015).
[23]G. Gariepy, N. Krstajić, R. Henderson, C. Li, R. R. Thomson, G. S. Buller, B. Heshmat, R. Raskar, J. Leach, and D. Faccio, "Single-photon sensitive light-in-flight imaging," Nat. Commun. **6**, 6021 (2015).
[24]H. K. Chandrasekharan, F. Izdebski, I. Gris-Sánchez, N. Krstajić, R. Walker, H. L. Bridle, P. A. Dalgarno, W. N. MacPherson, R. K. Henderson, T. A. Birks, and R. R. Thomson, "Multiplexed single-mode wavelength-to-time mapping of multimode light," Nat. Commun. **8**, 14080 (2017).
[25]S. Mukherjee, H. K. Chandrasekharan, P. Öhberg, N. Goldman, and R. R. Thomson, "State-recycling and time-resolved imaging in topological photonic lattices," Nat. Commun. **9**, 4209 (2018).
[26]W. Becker, *Advanced Time-Correlated Single Photon Counting Techniques* (Springer, Berlin, Heidelberg, 2005).
[27]D. N. Payne and A. H. Hartog, "Determination of the wavelength of zero material dispersion in optical fibres by pulse-delay measurements," Electron. Lett. **13**, 627–629 (1977).
[28]J. Zhang, Z. Wu, T. Huang, X. Shao, and P. Shum, "Modes effective refractive index difference measurement in few-mode optical fiber," in *International Conference on Materials for Advanced Technologies (ICMAT2015), 4th Photonics Global Conference 2015* [Proc. Eng. **140**, 77–84 (2016)].
[29]K. Ehrlich, A. Kufcsák, N. Krstajić, R. K. Henderson, R. R. Thomson, and M. G. Tanner, "Fibre optic time-resolved spectroscopy using CMOS-SPAD arrays," Proc. SPIE **10058**, 95–102 (2017).
[30]K. Ehrlich, A. Kufcsák, S. McAughtrie, H. Fleming, N. Krstajic, C. J. Campbell, R. K. Henderson, K. Dhaliwal, R. R. Thomson, and M. G. Tanner, "pH sensing through a single optical fibre using SERS and CMOS SPAD line arrays," Opt. Express **25**, 30976–30986 (2017).
[31]N. Krstajić, J. Levitt, S. Poland, S. Ameer-Beg, and R. Henderson, "256 × 2 spad line sensor for time resolved fluorescence spectroscopy," Opt. Express **23**, 5653–5669 (2015).
[32]A. Kufcsák, A. Erdogan, R. Walker, K. Ehrlich, M. Tanner, A. Megia-Fernandez, E. Scholefield, P. Emanuel, K. Dhaliwal, M. Bradley, R. K. Henderson, and N. Krstajić, "Time-resolved spectroscopy at 19,000 lines per second using a CMOS SPAD line array enables advanced biophotonics applications," Opt. Express **25**, 11103–11123 (2017).
[33]H. K. Chandrasekharan, "Observing mode-dependent wavelength-to-time mapping in few-mode-fibers using TCSPC-SPAD arrays," Heriot-Watt University (2019), available at https://doi.org/10.17861/4248c758-58a6-47b4-b509-3d55a8aaff84.